Workshop on Material Appearance Modeling (2013)
H. Rushmeier and R. Klein (Editors)

DOME II: A Parallelized BTF Acquisition System

Christopher Schwartz, Ralf Sarlette, Michael Weinmann and Reinhard Klein

University of Bonn, Germany

Abstract

Bidirectional Texture Functions (BTFs) provide a realistic depiction of the appearance of many real-world materials as they contain the spatially varying light scattering behavior of the material surface. Since editing of existing BTF data is still in its early stages, materials have to be measured from real-world samples. In contrast to the related Spatially Varying BRDFs (SVBRDFs), the reflectance information encoded in a BTF also includes non-local scattering effects and therefore does not obey energy conservation or reciprocity. While this higher degree of freedom also contributes to an increased realism, it inadvertently calls for an extensive measurement of reflectance samples, as many regularization approaches from BRDF measurement do not apply. In this paper, we present an automated, parallelized, robust, fast and transportable setup for the acquisition of BTFs from flat samples as well as 3D objects using camera and light arrays: the DOME II. In contrast to previous camera array approaches, the present setup, which is comprised of high-quality industry grade components, overcomes several issues regarding stability, reliability and precision. It achieves a well balanced state-of-the-art acquisition performance in terms of speed and quality at reasonable costs.

1. Introduction

The accurate digital reproduction of surface material appearance is of great importance in a wide range of applications in industry and cultural heritage, such as product design, virtual prototyping, advertisement and entertainment or the creation of virtual surrogates of valuable objects. The most faithful reproduction of material characteristics can be obtained from measurements of real-world exemplars.

Several acquisition setups have been proposed for this task. They mainly differ in the complexity of the material effects that can be reproduced. The characteristic appearance of a material is the result of light interacting with the surface. While measuring this interaction in its most general case, the 12D Bidirectional Surface Scattering Reflectance Distribution Function (BSSRDF), is prohibitively costly, the 6D Bidirectional Texture Function (BTF) lends itself as a realistic approximation. It explicitly includes perceptually important non-local scattering effects, such as shadows, inter-reflections, sub-surface scattering or masking, as an important contribution to a material's characteristic appearance. As a consequence, BTFs are the technique of choice for the faithful digital reproduction of many real-world materials.
The BTF is defined as a function $\rho(\mathbf{x}, \omega_i, \omega_o)$, with $\mathbf{x}$ denoting the position on the surface and ω_i and ω_o being the light and view direction. A key factor to the realistic impression is the ability to directly render using the acquired data instead of fitted models, given a sufficiently dense sampling.

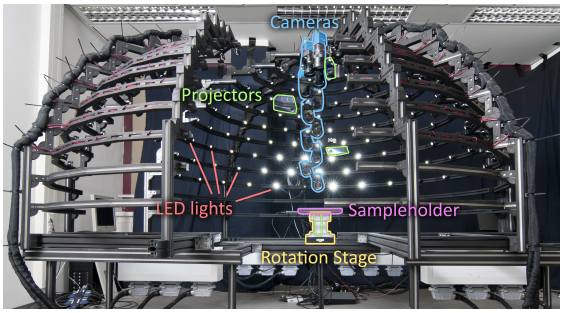

Figure 1: The DOME II BTF acquisition setup. One quarter has been slid open to expose the view on the inside.

In this paper, we will present a new hardware design and the necessary calibration and processing procedures for the acquisition of BTFs. Our setup is intended to be widely applicable, which requires a "brute-force" sampling of all 6 dimensions. In addition, we can also robustly and precisely reconstruct 3D geometries. This allows for the dedicated acquisition of mesoscopic material geometry, e.g. displacement maps, as well as capturing shape and reflectance of complete 3D objects. To make our setup practically feasible,

DOI: 10.2312/MAM.MAM2013.025-031

we find a compromise between sampling resolution, measurement quality and speed as well as reliability and costs of the employed hardware.

2. Related Work

A recent detailed overview of setups for capturing material appearance can be found in [HF11]. In the following, we will briefly summarize those approaches most closely related to our designated purpose of measuring BTFs. A more detailed comparison can be found in the appendix.

Gonioreflectometer Setups: In the first BTF measurement device proposed in [DNVGK97], a flat material sample is mounted on a robotic arm which changes its pose relative to a fixed light source. The sample is captured by a camera being placed at seven different positions during measurement. Due to mechanical constraints and the need for manual interaction, only a sparse set of directions was captured and anisotropy was handled insufficiently. More recent works [SSK03, HFV12] presented automated versions of a similar setup that allow for much higher direction samplings and also account for anisotropy. However, the involvement of moving parts in these setups impacts both accuracy and measurement time. Every single picture has to be carefully calibrated e.g. by using markers next to the material sample.

Kaleidoscopes: In kaleidoscope-based approaches [HP03, IRM*12], a clever arrangement of mirrors provides a set of recursive inter-reflections that present all views to the camera at once. Using a digital projector in combination with a beam-splitter, different light directions can be generated utilizing the same inter-reflection paths as the view directions. Therefore, all parts of the setup remain fixed. Although the light directions still have to be sampled sequentially, view directions and spatial domain are captured in parallel, allowing a considerable speed-up of the measurement compared to gonioreflectometer devices. However, these setups involve a trade-off between spatial resolution and the number of possible direction combinations and require a highly accurate calibration. In [IRM*12], the authors demonstrate that reflectance can be captured from 3D surfaces using this approach.

Camera Arrays: A different way towards reduction of measurement time can be found in using arrays of light sources and cameras. In [MMS*04], a highly-parallelized dome setup with 151 digital consumer cameras mounted on a hemisphere above the material sample is presented. Using this setup, BTFs can be measured without any moving parts. All cameras take pictures at the same time, capturing all view directions in parallel without sacrificing spatial resolution. In [SWRK11], the setup is extended with projectors to facilitate the acquisition of BTFs from 3D surfaces.
The approach followed in this paper falls into this category as well. However, our setup has a reduced number of cameras which is compensated by additionally using a rotation stage. A similar trade-off was made by Köhler et al. [KNRS13] for capturing the reflectance on 3D objects with a full-spherical arrangement. In contrast to our approach, their setup still requires to move the cameras, which is observed to be an obstacle for a stable calibration.

3. Hardware Design

Our setup consists of a dome structure with industrial digital video cameras, a precision rotation stage and LED lamps. Light-sources and cameras are rigidly aligned and stay at fixed positions during the whole measurement. The rotation stage, which is used for capturing anisotropic materials, is the only movable part. Yet, it is fast, accurate and reliable.
In the following, we will provide a more detailed discussion of the individual hardware components.

Gantry: The gantry should meet the following requirements: (i) sufficient space for all components, (ii) a hemisphere diameter that facilitates sample size, focus distance and depth-of-field (iii) stable and rigid mounting of the hardware, (iv) a compact and light-weight construction for being transportable, (v) being openable for maintenance access, and (vi) allowing the installation of an automatic feed for samples. Our setup, illustrated in Figure 1, meets these requirements by a dismountable, light-weight hemispherical structure. The diameter of 2 m provides a sufficient distance to the material samples. The hemisphere is organized in rings at inclination angles $\theta = 0^\circ, 7.5^\circ, \ldots, 90^\circ$ on which cameras, LEDs and projectors are installed and which are held in place by struts. There is enough space to let an automatic feed pass through below the ring at 90° inclination.

Cameras: We use eleven cameras that are mounted on an arc above the material sample at different inclination angles $\theta_o = 0^\circ, 7.5^\circ, \ldots, 75^\circ$. When turning the rotation stage in steps of 15° to different azimuth angles φ_o, we are able to sample the view directions $\omega_o = (\theta_o, \varphi_o)$ in a dense, regular grid of 11×24 with some degree of parallelism.

We employ `SVS Vistek SVCam CF 4022COGE` cameras (CCD-sensor with CFA, 2048×2048 pixels, 12 bit/pixel, 8 FPS). The large sensor (16×16 mm) provides for a high light sensitivity at low noise levels. To account for the high dynamic ranges (HDR) found in material reflectance, the electronic shutter has customizable exposure times from $50\,\mu$s to ∞. The raw-data is transmitted via Gigabit-Ethernet, which also serves as the control-connection. All eleven cameras are operated by a single computer, avoiding any synchronization issues or the fragmented storage of the measured data. We sample the BTF at three spectral bands (RGB), given by the Bayer color-filter-array (CFA) of the camera.

The cameras are equipped with high-quality `ZEISS Makro Planar T*2 ZF-I` prime lenses. A set of lenses

with 100 mm focal-length is employed for measuring BTFs from flat material samples, offering about 380 DPI spatial resolution. For measuring BTFs on larger 3D objects, a second set with 50 mm is available. We use a fixed aperture of f/19 on all lenses to have a sufficiently large depth-of-field and focus on the center of the DOME II. Both settings are fixated using locating screws, which vastly improves stability of calibration throughout multiple measurements.

Light Sources: For sampling the light directions $\omega_i = (\theta_i, \varphi_i)$, we equipped the full hemispherical gantry with a light dome of individually switchable LED lamps. This avoids the use of movable parts for the light sources.

188 LEDs are placed evenly spaced on the rings at 0° to 75° inclination. Care has been taken that the positions are in alignment under rotations φ_i in increments of 15°, also leading to a regular grid of 11×24 light directions. To facilitate the usage of Helmholtz reciprocity for 3D reconstruction (see for example [WRO*12]), the lights are arranged symmetrically around the cameras and thus allow the formation of reciprocal pairs for rotations of $n \cdot 15^\circ + 7.5^\circ$. Another 10 light sources are arranged to emit into the perfect reflection direction of the cameras at 7.5° to 75°, allowing a better observation of specular effects.

We selected `Barthelme Bari DC` show-case LED lamps (2.5 W, 215 lm, phosphor coated, 6000 K) which emit a broad spectrum, matching the cameras' CFAs, and come with optics to concentrate the light on a single spot, i.e. the material sample. All LEDs are from one batch to avoid differences in brightness and spectra. Additionally, after switching on an LED we wait for it to reach a stable operating conditions and thus reproducible characteristics.

Projectors: To facilitate the measurement of BTFs on 3D objects instead of planar samples, the Dome II setup is equipped with four `LG HS200G` digital projectors (800×600 pixels, LED-DLP, 200 lm) for reconstructing the 3D geometry via structured light. The projectors are installed next to the camera arc at different inclination angles from 0° to 90°. They are small, light-weight and have a sufficiently near projection distance and wide depth-of-field for our use-case.

We observed that after turning on, the projection drifts and takes up to 15 minutes to stabilize. Additionally, the colors alternate periodically with a slightly irregular pattern, making it necessary to synchronize exposure with projector frequency in order to avoid color shifts. Due to these shortcomings, we plan to replace the projectors with `CASIO XJ-A141` (1024×768 pixels, LED-DLP, 2,500 lm). In our first experiments, these models did not exhibit a drift and also facilitated shorter synchronization times.

Turntable & Sampleholder: The sample is fixated by a blackened sampleholder (Fig. 2c) and placed on a `Newport URS-150BCC` computer controlled precision rotation stage

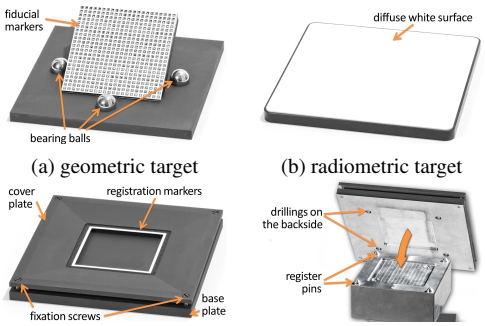

(a) geometric target (b) radiometric target

(c) sampleholder (d) fixation on turntable

Figure 2: The custom-tailored calibration targets (a) and (b), the sampleholder (c) and the fixation mechanism (d).

with a guaranteed uni-directional repeatability of 0.002°. The detachable sampleholder is held in place by four register pins (Fig. 2d). A cover plate with additional registration markers is put on top of the material sample and provides an adjustable clamping pressure via four screws. The visible area of the material sample is 7.5×7.5 cm. 3D objects are placed on the sampleholder without the cover plate, which requires a precise calibration of the device.

4. Calibration, Measurement & Processing

One advantage of the proposed setup is the fact that all parts, except the sampleholder and turntable, are rigidly affixed to each other. Still, since the turntable shows a high accuracy and the sampleholder is held in place without mechanical play, we also consider their positions reliable. This allows to perform one thorough calibration that is then used for several measurements.

Calibration: The geometric calibration of all parts is performed utilizing a custom-tailored target (Fig. 2a) that features a 10×10 cm plate with 484 fiducial markers [MS13] and four polished bearing balls. Markers and balls have a known size and position. The target is placed on the turntable instead of the sampleholder and rotated to be captured in various different poses. The cameras are calibrated via the fiducial markers, employing Zhang's algorithm [Zha00] with a successive sparse bundle adjustment [LA09]. The resulting re-projection errors are 0.16 pixels on average, which corresponds to a spatial error of $11\,\mu$m and an angular error of 0.001° in the view direction. The turntable's axis and center of rotation are obtained from the triangulated 3D locations of the markers. After calibration, different poses are brought into alignment with an average deviation of 0.003°.
For calibrating the light positions, we identify for each light its reflection-point in all four bearing balls. Using these features and a good initial estimate for the bearing balls' positions and radii, we can compute the reflection rays via ray-tracing and triangulate the LED position from them. Afterwards, we perform a non-linear optimization on all LEDs

and the sphere positions simultaneously to reduce the reprojection error of the observed reflections. Here, we can report an average error of 0.4 px, corresponding to an angular error of about 0.08° for the light directions.

In addition to the geometric calibration, a radiometric calibration is performed. First, we take a set of *dark-frames*, i.e. raw images of a completely unlit scene, with all cameras and at different exposure times. Then, we compute the cameras' response functions by taking an exposure series and employing the method of Robertson [RBS03]. Finally, a *white-frame* for every camera and light combination is captured from a white-target made from `SphereOptics ZENITH UltraWhite` (Fig. 2b) that is put in place on the rotation stage. Our target is almost perfectly lambertian with an albedo of 99% in the visible spectrum.
Using *dark-frame subtraction* and the inverse response function, we eliminate sensor-bias as well as dead- or hot-pixels and obtain linear values proportional to radiance. Dividing this values by the values in the corresponding white-frame we obtain the reflectance $\rho\,[\mathrm{sr}^{-1}]$ (see appendix).

Measurement: We execute our measurement procedure with the goal to minimize the time spent waiting for slow operations to finish. Given a planar sample, we first move the rotation stage to the desired pose. Then we consecutively switch through the light-sources, always illuminating the sample with exactly one LED, and for each one take a HDR exposure series with all cameras simultaneously. For reconstructing 3D geometry, we also perform a structured light measurement. Here, we first switch on the projector and then rotate through the desired poses. For every rotation we capture a 2D pattern sequence with all cameras.

The raw images are captured directly onto a clean harddisk to avoid loosing write-speed due to file-system fragmentation. Still, depending on the exposure time the data rate can reach 528 MB/s and the disk's write-speed becomes a limiting factor for the measurement performance. Therefore, we employ a write-queue in RAM which is worked off during more time-consuming operations.
Depending on the dynamic range of the material, a full anisotropic BTF measurement takes between 4 and 10 hours. Additionally acquiring the 3D geometry takes another 1.5 to 3 hours. Instead, capturing a flat isotropic material will merely take 15 to 30 minutes in total. A more detailed discussion on measurement times can be found in the appendix.

Postprocessing: To allow efficient storage, compression and rendering, every single HDR image of the captured BTF data is first rectified by computing and applying the respective projection onto a reference geometry. Conventionally, this is a plane, but could also be a heightmap or the parametrized 3D geometry of an object, which we reconstruct from the structured light. As a result we obtain 52,272 rectified images. However, for planar materials, ω_i and ω_o vary by about 4.3° over these image. In the case of 3D objects, the directions in an image are completely arbitrary. For compression and rendering, an evenly-spaced, dense sampling of the angular domain would be desirable. Therefore, we perform an angular resampling on the rectified images employing the method described in [SWRK11].

5. Conclusion and Future Work

We have presented a measurement device that is capable of capturing BTFs densely and unbiased in all six dimensions. Our setup yields a reasonable compromise between acquisition speed, processing and calibration effort, costs and quality as well as general robustness. In contrast to most other setups, the hardware is constituted from high-quality industry parts that we selected for reliability and endurance. This way, our setup is fit to serve as a mass acquisition device for practical application even outside a lab environment.
Most of the money is spent on the high-quality cameras and lenses, which make up the heart of an optical measurement instrument. However, in turn we limit ourselves to eleven cameras and alleviate the hereby induced issues of speed and registration by employing a full light-dome, a precision rotation stage and a thorough calibration and post-processing. As a result, we achieve measurement times that lie in the middle between the latest dome setups and gonioreflectometers, while at the same time capturing 2.2 or 8 times as many directions, respectively. The spatial resolution, sample sizes and 3D abilities are on the state of the art as well. To the best of our knowledge, our setup is the first of its kind that is specifically designed to be easily transportable and can be assembled and calibrated in 16 hours.

As a next step, we plan to extend the setup with an additional camera and another ring of LEDs to better capture the important reflection effect predicted by the Fresnel-equations. Further plans include improving the measurement speed and calibrating the CIE color-profile of our device for colorimetric correct material visualization.

References

[DNVGK97] DANA K. J., NAYAR S. K., VAN GINNEKEN B., KOENDERINK J. J.: Reflectance and texture of real-world surfaces. In *CVPR* (1997), pp. 151–157. 2, 6

[HF11] HAINDL M., FILIP J.: Advanced textural representation of materials appearance. In *SIGGRAPH Asia Courses* (2011), pp. 1:1–1:84. 2

[HFV12] HAINDL M., FILIP J., VÁVRA R.: Digital material appearance: the curse of tera-bytes. *ERCIM*, 90 (2012), 49–50. 2, 6

[HP03] HAN J. Y., PERLIN K.: Measuring bidirectional texture reflectance with a kaleidoscope. In *SIGGRAPH* (2003), pp. 741–748. 2, 6

[IRM*12] IHRKE I., RESHETOUSKI I., MANAKOV A., TEVS A., WAND M., SEIDEL H.-P.: A kaleidoscopic approach to surround geometry and reflectance acquisition. In *CVPRW* (2012), pp. 29–36. 2, 6

[KNRS13] KÖHLER J., NOLL T., REIS G., STRICKER D.: A full-spherical device for simultaneous geometry and reflectance acquisition. In *WACV* (2013), pp. 355–362. 2, 6

[LA09] LOURAKIS M. A., ARGYROS A.: SBA: A Software Package for Generic Sparse Bundle Adjustment. *ACM TOMS 36*, 1 (2009), 1–30. 3

[MMS*04] MÜLLER G., MESETH J., SATTLER M., SARLETTE R., KLEIN R.: Acquisition, synthesis and rendering of bidirectional texture functions. In *Eurographics STAR* (2004), pp. 69–94. 2, 6

[MS13] MUÑOZ-SALINAS R.: Aruco: Augmented reality library from the university of cordoba. Website, 2013. Available online at http://sourceforge.net/projects/aruco/files/1.2.4/; visited on May 3rd 2013. 3

[RBS03] ROBERTSON M. A., BORMAN S., STEVENSON R. L.: Estimation-theoretic approach to dynamic range enhancement using multiple exposures. *JEI 12*, 2 (2003), 219–228. 4

[SSK03] SATTLER M., SARLETTE R., KLEIN R.: Efficient and realistic visualization of cloth. In *EGSR* (2003), pp. 167–177. 2, 6

[SWRK11] SCHWARTZ C., WEINMANN M., RUITERS R., KLEIN R.: Integrated high-quality acquisition of geometry and appearance for cultural heritage. In *VAST* (2011). 2, 4, 6

[WRO*12] WEINMANN M., RUITERS R., OSEP A., SCHWARTZ C., KLEIN R.: Fusing structured light consistency and helmholtz normals for 3d reconstruction. In *BMVC* (2012). 3, 7

[Zha00] ZHANG Z.: A flexible new technique for camera calibration. *PAMI 22* (2000), 1330–1334. 3

Appendix 1: Problem Definition

Consider the BTF as a function

$$\begin{array}{rccc} \rho: & \mathbb{R}^2 \times \Omega \times \Omega & \mapsto & \mathbb{R}^n \\ & (\mathbf{x}, \omega_i, \omega_o) & \rightarrow & \left(\frac{\partial L_o(\mathbf{x},\omega_o)}{\partial E_i(\omega_i)}\right)_\lambda \end{array}, \qquad (1)$$

giving the ratio of the differential incident irradiance ∂E_i from direction ω_i to the differential outgoing radiance ∂L_o at position $\mathbf{x} \in \mathbb{R}^2$ on the material sample into direction ω_o, with $\omega_i = (\theta_i, \varphi_i) \in \Omega$ and $\omega_o = (\theta_o, \varphi_o) \in \Omega$ being directions in the hemisphere $\Omega = [0, \frac{\pi}{2}] \times [0, 2\pi]$ above the material sample. The ratio is defined for a set of n discrete wavelength-bands $\{\lambda\}_n$. In contrast to a full BSSRDF, the simplifying assumptions are made that ρ does neither show fluorescence nor phosphorescence and that the incoming light from direction ω_i is the same for all points on the material sample, allowing to account for sub-surface light-transport using only an exit position $\mathbf{x}$.

Appendix 2: Radiometric Correction

From the Rendering Equation we get

$$L(\mathbf{x}, \omega_o) = \int_\Omega \rho(\mathbf{x}, \omega_i, \omega_o) L_i(\mathbf{x}, \omega_\mathbf{i}) \cos\theta_i \, d\omega_i.$$

Let us consider a specific pixel in the camera's image. This way, we can assume the outgoing direction ω_o and the position on the surface $\mathbf{x}$ to be constant and dismiss them in our considerations of the image formation process. Then the radiance $L\,[\mathrm{Wm}^{-2}\mathrm{sr}^{-1}]$ up to a proportionality factor α is obtained from a camera-pixel's value by subtracting the dark-frame and applying the inverse response-function.

Consider the white-target to be a perfectly lambertian object with known albedo a. Then ρ is simply $\frac{a}{\pi}\,[\mathrm{sr}^{-1}]$ and αL_w is formed by

$$\begin{aligned} \alpha L_w &= \alpha \int_\Omega \frac{a}{\pi} L_l(\omega_i) \cos\theta_i \, d\omega_i \\ &= \alpha \frac{a}{\pi} \int_\Omega L_l(\omega_i) \cos\theta_i \, d\omega_i. \end{aligned}$$

Here, $L_l\,[\mathrm{Wm}^{-2}\mathrm{sr}^{-1}]$ denotes the (unknown) radiance coming from the scene due to light-source l being switched on.

Furthermore, we know that the irradiance $E_w\,[\mathrm{Wm}^{-2}]$ at the observed point on the surface must be

$$\begin{aligned} E_w &= \int_\Omega L_l \cos\theta_i \, d\omega_i \\ &= \frac{\pi}{a} L_w. \end{aligned}$$

Now, consider the measurement of an arbitrary unknown reflectance function $\rho(\mathbf{x}, \omega_i, \omega_o)\,[\mathrm{sr}^{-1}]$. Let us further assume that the light illuminating the observed surface point covers only a small solid angle ω and ρ is constant over ω for fixed $\mathbf{x}$ and ω_o. This assumption is reasonable for a single LED emitter at a large enough, which can be considered to be almost a point light. Then the image formation process leading to measured radiance αL_m for a single camera pixel (constant view direction and point on surface) and single LED (constant reflectance behavior) can be written as

$$\begin{aligned} \alpha L_m &= \alpha \int_\Omega \rho L_l(\omega_i) \cos\theta_i \, d\omega_i \\ &= \alpha\rho \int_\Omega L_l(\omega_i) \cos\theta_i \, d\omega_i \\ &= \alpha\rho E_w. \end{aligned}$$

Thus, we can determine the value of ρ for the fixed sample $(\mathbf{x}, \omega_o, \omega_i)$ as follows

$$\rho = \frac{\alpha L_m}{\alpha E_w} = \frac{a}{\pi} \frac{\alpha L_m}{\alpha L_w}$$

with αL_m and αL_w being the measured values in the image taken during measurement and its corresponding white-frame, respectively.

Appendix 3: Setup Comparisons

Paper	sample size [cm^2]	spatial resolution [DPI]	direction samples	measurement time [h]	# physical cameras	3D objects
Gonioreflectometers						
[DNVGK97]	100	114	205-410	1 – 2	1	no
[SSK03]	64	200	6,561	14	1	no
[HFV12]	196	1000	6,561	13	1	no
Kaleidoscopes						
[HP03]	33.64	85	484-6,241	1	1	no
[IRM*12]	?	?	120	71	1	yes
Camera arrays						
[MMS*04]	100	280	22,801	?	151	no
[SWRK11]	100	480	22,801	2-3	151	yes
[KNRS13]	?	?	?	?	7	yes
DOME II	56.25	380	52,272	4-10	11	yes

All figures are taken from the cited documents and other publicly available sources, such as websites describing the device. It might be possible that some numbers have been improved since their original publication. The number of actually employed physical cameras is given as a hint to estimate the costs and complexity of a setup.

Appendix 4: Measurement Details

The measurement times and number of captured images depend on the dynamic range of the material and hence the number of required images in an exposure series. Let $\mathrm{Exp}_1, |\mathrm{Exp}_1| = E_1$ denote the set of exposure times we take for the BTF measurement and $\mathrm{Exp}_2, |\mathrm{Exp}_2| = E_2$ denote the

set of exposure times we take for capturing the structured light patterns.

For measuring a BTF we perform $R_1 = 24$ rotations, in each rotation switch on and off $L = 198$ lights, and capture a HDR exposure series with E_1 exposures on all $C = 11$ cameras simultaneously. For measuring a 3D geometry, we switch on and off $P = 4$ projectors, perform R_2 rotations, project $N = 42$ patterns and capture an HDR exposure series with E_2 exposures on all $C = 11$ cameras simultaneously. Each captured image is 2048×2048 pixels á 12 Bit (6 MB).

Files and Filesize: For BTFs we capture $R_1 \cdot L \cdot C \cdot E_1$ raw images, which constitute $R_1 \cdot L \cdot C = 24 \cdot 198 \cdot 11 = 52{,}272$ rectified HDR images. Usually, $E_1 = 2 \ldots 4$, thus a raw BTF measurement has between $2 \cdot 52{,}272 = 104{,}544$ and $4 \cdot 52{,}272 = 209{,}088$ images, occupying 612.6 GB-1.2 TB of disk space. The full 7.5×7.5 cm at 380 DPI will result in $\left(7.5\,\text{cm} \cdot \frac{380\,\text{DPI}}{2.54\,\frac{\text{cm}}{\text{inch}}}\right)^2 \cdot 52{,}272 \cdot 2\,\text{B}) = 122.5\,\text{GB}$ for the rectified images (in 16 Bit half-precision floating point).
For the structured light images, we choose R_2 depending on the geometric complexity. Usually $R_2 = 8$ and $E_2 = 1 \ldots 3$. Thus, we have $R_2 \cdot P \cdot N \cdot C \cdot E_2 = 8 \cdot 4 \cdot 42 \cdot 11 \cdot E_2 = 14{,}784$ to 44,352 images, occupying 86.6 GB to 260 GB, from which a 3D geometry is reconstructed (see [WRO*12]).

Measurement Time: The total measurement time T can be expressed by three parts: time spent capturing images T_c, time spent waiting for hardware operations to finish T_h and the time required to write the images onto the disk T_d: $T = \max(T_c + T_h, T_d)$. T_d and $T_c + T_h$ can be considered separately, since we employ a write-queue in RAM. $T_d^{\text{btf}} = \frac{6\,\text{MB} \cdot R_1 \cdot L \cdot C \cdot E_1}{D}$ and $T_d^{\text{3D}} = \frac{6\,\text{MB} \cdot R_2 \cdot P \cdot N \cdot C \cdot E_2}{D}$, where D denotes the average disk's write speed. In most of our measurements, this was about $D = 40\,\text{MB/s}$.
$T_c^{\text{btf}} = \sum_{t \in \text{Exp}_1} (t + 3 \cdot 125\,\text{ms}) \cdot R_1 \cdot L$ and $T_c^{\text{3D}} = \sum_{t \in \text{Exp}_2} (t + 3 \cdot 125\,\text{ms}) \cdot R_2 \cdot P \cdot N$. To improve the CCD-clearing performance, we actually take 3 images per shot (two with $50\mu s$ and one with the target exposure). Each time we have to wait 125 ms, due to the cameras' frame-rate of $8s^{-1}$. Note that the factor C is not included in the capture-times, since the cameras all capture in parallel.
Finally, $T_h^{\text{btf}} = R_1(9\,\text{s} + 250\,\text{ms} \cdot L)$ and $T_h^{\text{3D}} = 15\,\text{min} \cdot P + R_2(9\,\text{s} + 100\,\text{ms} \cdot P \cdot N)$. In both cases we assume that we have to wait 9 s for the turntable to reach its new pose. In the BTF case, we wait a warm-up delay of 250 ms after switching on each light in order for the spectral characteristics to stabilize (see Figure 3). In the 3D acquisition case, we wait 15 min per projector for the projection to stop shifting. As mentioned before, we plan to replace the current projectors with new models, to avoid this unnecessary delay. Additionally, we cautiously wait 100 ms after each change of pattern for the projector to actually display the new one.

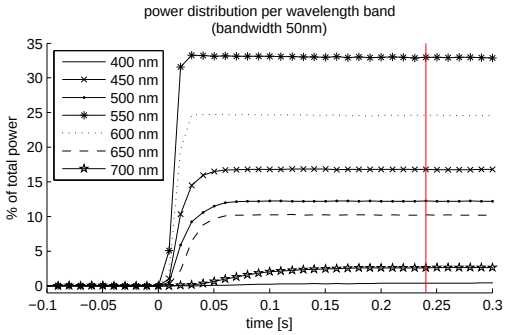

Figure 3: A time series of the spectral power distribution of our LED light-sources. The light-source is turned on at time $t = 0$ s. Note that higher wavelengths take more time to reach their final power output. The vertical red line at $t = 240$ ms marks the time at which the 99^{th} percentile of the final power is reached. After this point we consider the spectral characteristics to be stable.